

Bending Modes for Active Optics

Byron Smith^{*a}, Brian Cuerden^b

^aX Double Dot, 723 W Aspen Ave. #A, Flagstaff, AZ 86001;

^bUniversity of Arizona Steward Observatory, 933 N Cherry Ave., Tucson, AZ 85721

ABSTRACT

While the concept of wavefront decomposition is a foundation of active optics systems, the choice of basis functions for mirror figure control is divided. The common functions are Zernike polynomials, ubiquitously used for wavefront descriptions, and bending (also called minimum energy or vibration) modes which offer optimal performance. We present a look at the comparative performance between the two approaches, and discuss an implementation approach which seeks to combine much of the analytic and interface simplicity of Zernike polynomials with the improved performance of bending modes.

Keywords: Active optics, bending modes, figure control, basis function

1. INTRODUCTION

Active optics systems measure the delivered wavefront and utilize feedback control to improve the overall system performance, by adjusting one or more actively supported optical elements to minimize errors. In large astronomical telescopes, typically the primary mirror figure and secondary mirror alignment are actively controlled in this manner. The wavefront may be measured by a number of possible techniques, with the Shack-Hartmann method being the most common.

The translation between the raw wavefront error measurement and the resulting mirror support adjustments to minimize the errors is a key part of any active optics system; and an intermediate description of the wavefront error as a linear combination of basis functions helps facilitate this process. The basis functions commonly chosen are either Zernike polynomials¹ or bending modes of the (actively supported) primary mirror. An excellent discussion of basis functions and active optics in general can be found in Noethe's 2002 summary article².

The motivation for writing this paper arose from discussions between the author and a colleague regarding the use of Zernikes versus bending modes as active optics basis functions. To the author, a mechanical engineer, bending modes seemed the natural choice, due to their theoretically superior performance and resemblance to the physical system being controlled. To the colleague, an optical engineer, Zernikes seemed the better choice, as the universal language of wavefronts and corresponding advantages as a system interface.

In a modern astronomical telescope, both performance and system complexity are important considerations; but lacking a direct performance comparison between the two approaches it is impossible to make an informed trade. Although modal stiffness and correction residuals are both much lower for bending modes (over an order of magnitude for both in the case of the DCT), these large reductions apply to small errors and don't provide an adequate comparison. What is needed is an end-to-end performance comparison in terms of mirror surface error.

We present here a comparison using the Discovery Channel Telescope (DCT) primary mirror (M1) as an example. The DCT M1 is a ULE thin meniscus; of 4.3m outer diameter, 1.1m inner diameter, 100mm thick and a nominal radius of curvature of 16m. The mirror is supported by 120 active axial supports and 36 lateral supports³, and is fairly representative of large meniscus mirrors both existing and currently planned.

We also address the system interface aspect of using bending modes as basis functions, and present a method of using bending modes for mirror figure control while retaining a Zernike interface to the wavefront sensor.

^{*}bsmith@xdoubledot.com; phone 1 928 225-0788; www.xdoubledot.com

2. PERFORMANCE COMPARISON

2.1 Scope

Evaluate the DCT primary mirror support performance for both Zernike and bending mode shapes as figure control basis functions, and compare the results.

2.2 Discussion

The 120 axial actuators can bend in 117 unique shapes along with piston, tip and tilt rigid body motions. These shapes can be calculated in a ranked order from the shapes most easily bent in to the shapes that are the most difficult to bend in. For the DCT mirror, these ranked shapes can be computed using a free-free modal analysis in which the mirror mass is replaced by axial mass at each axial actuator (the ANSYS mass element allows X, Y and Z mass to be specified separately). The advantage of these shapes is that they can be bent in perfectly by the actuators (no residual errors). Normal practice is to select some number of the low order shapes to be used for mirror correction. The low order shapes are most easily bent in so they are most likely to be present in the operational mirror, in fact, mirror figure is sensitive to errors in the axial support forces so a major contributor to figure errors, axial support force errors, can naturally be corrected using bending shapes.

The support system analysis included shear and moment errors at the axial actuators and extraneous forces from the lateral support system. None of these can be perfectly corrected by the axial actuators. The support analysis could be expected to favor the bending shapes because it includes components bent in by axial error forces of the axial actuators. Included are low order distributions of axial forces that naturally produce relatively large amounts of the corresponding low order bending shapes. It is, however, realistic to expect that such low order axial force distributions exist and that we should prefer a mirror correction system that can readily correct the induced errors.

2.3 Procedure

The DCT primary mirror support analysis evaluates 114 load sets. Gravity effects are excluded here because the loads are initially set by analysis to the optimum values so the correction system can only see changes from that condition. Many of these load cases are representative samples of multiple error sources. For example, there are 36 actuators in the outer ring but the six possible force errors are only evaluated at one conservatively selected location. These results are added into the total compilation 36 times. The force error estimates consider how much is correctable and how much is not correctable. An example of a correctable component is one that is caused by an installed position error. The position error is always present so its effect will be measured and can be corrected. An uncorrectable error is one that might change between successive surface measurements. Friction forces are always assumed to be uncorrectable.

The uncorrectable surface distortions are excluded from this analysis since their effect is present in both cases. This does mean that we are looking at a fraction of the support error budget as shown in Table 1 where the total rms distortion is 121.9 nm-rms and 0.051 sec-rms including un-correctable terms of which only 13.9 nm-rms and .028 sec-rms is from the residual after correction using bending shapes. The amount of correctable distortion before correction was 620 nm-rms and 0.23 arc-sec rms (231 nm-rms and 0.14 sec-rms excluding astigmatism which is readily correctable using either set of shapes). A relatively large fraction of the net slope error comes from the residuals of correctable errors and there is a significant difference between using bending shapes (0.028 sec-rms) and Zernikes (0.041 sec-rms). Note that "correctable" does not mean the effect can be fully removed. It only means we can measure it and try to bend it out, hence we have a residual of the original distortion that varies depending on the number of shapes we use and the shapes we choose to use.

The values cited above and listed in Table 1 are calculated by subtracting bending or Zernike shapes from individual load cases and RSS'ing the results to arrive at a total distortion. This procedure is consistent with the statistical principles being employed to combine statistically independent randomly varying effects, some of which use sampled results applied multiple times. The downside to this approach is it makes it difficult to calculate the correction forces. A single distortion case was therefore created by summing all 114 load cases with each case multiplied by the square-root of the number of locations it represents. This gives a distorted shape that includes all the identified correctable effects but with some of the randomness eliminated. The results of subtracting 26 bending shapes or Zernikes from this case are similar to the RSS of individual results and are listed in Table 2. Note that the bending shape correction slope result is worse against this case while the Zernike slope result is about the same. Correction forces were of similar magnitudes whether Zernikes or bending shapes were used. Since the Zernike results are obtained by subtracting shapes that cannot

be perfectly bent in by the actuators, a final check was made to determine the magnitude of this effect. This task was accomplished by calculating the displacements for the sum of Zernikes that best corrects the mirror figure and calculating the net figure after a full correction (117 shapes obtained using a unit load at each actuator in turn). The results are listed in Table 2 and are nearly negligible.

Table 1. Comparison of Bending and Zernike Shape Corrections.

	Surface Distortion	
	nm-rms	sec-rms
Total, Correctable and Uncorrectable Effects		
using 26 DCT bending shapes	121.9	0.051
Total, Correctable Effects Only		
Using 26 DCT bending shapes	13.9	0.028
Using 26 Zernike terms	13.4	0.041

Table 2. Required Forces and Residual Error When Correcting Distortion Represented by the Sum of the Cases Considered in Table 1. The amount of correctable distortion before correction is 620 nm-rms and 0.23 sec-rms.

	Surface Distortion	
	nm-rms	sec-rms
Sum Correctable Displacements		
Correct using 26 DCT shapes	12.56	0.038
Correct using 26 Zernike terms	12.96	0.039
Residuals (when using Zernike shapes)		
Corrected using 26 Zernike terms	1.54	0.0079
Forces Required	Lbs rms	Lbs max
Correct using 26 DCT shapes	1.23	3.06
Correct using 26 Zernike terms	1.35	3.09

2.4 Performance Conclusions

We've generally found that most of the benefit comes from the lowest order shapes which can be bent in with relatively low force and with little residual error. The differences between Zernike and bending shape corrections tabulated above mainly represent differences between the higher order terms which represent a small part of the total distortion. In the case of the DCT primary, the total surface normal distortion is 122 nm-rms of which the repeating component after correction is only 14 nm-rms with Zernike and bending shape corrections being equally effective.

Slope errors attributable to repeating components are a large fraction of the total slope error with the bending shapes being noticeably more effective at 0.028 sec-rms compared to the Zernike correction at 0.041 sec-rms. Use of the Zernike correction would be expected to push the total error from 0.051 sec-rms to .059 sec-rms.

The degraded performance of the bending shapes when applied to the summed displacement case of Table 2 is probably the result of a failure to randomize the phasing of the individual load cases so the error forces are applied to a radial row of actuators resulting in large displacements at one location instead of smaller randomized displacements more or less uniformly distributed over the mirror. It is reasonable to expect the low-order bending shapes to be less effective on a shape that resembles distortion concentrated around a point than the actual distributed random distribution.

3. BASIS CONVERSION

While it is certainly possible to fit bending modes directly to the raw wavefront measurement (e.g. from Shack-Hartmann spot displacements⁴), if a sub-system boundary lies between the AOS controller and the wavefront sensor, as shown in Figure 1, a Zernike based interface may be desirable. Ubiquitously used for wavefront descriptions, Zernikes provide a ‘standard’ interface and allows simple interfacing with commercial wavefront sensors (or reusing existing software, as in the case of the DCT). Further, it allows the control and wavefront sensing functions to be designed independently, without knowledge of the other’s internal workings.

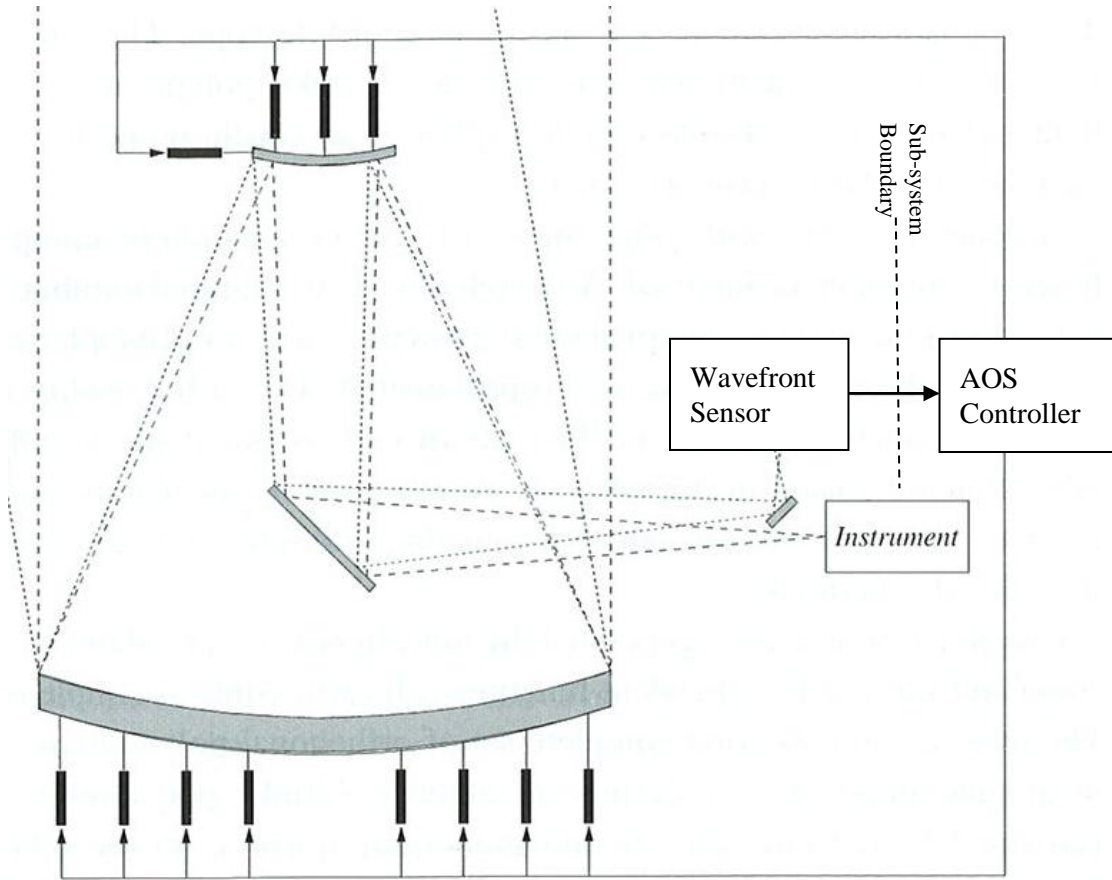


Figure 1. Schematic description of active optics system with boundary between wavefront sensor and AOS controller.
Adapted from Noethe (2002)².

3.1 Conversion Process

A straightforward conversion process allows utilizing bending modes for figure control. The goal of the conversion process is to take an input wavefront described in terms of Zernike coefficients, and to output a combination of low-order Zernike and bending mode coefficients, used for collimation and figure control, respectively. If the wavefront delivered to the focal plane is $W(\rho, \varphi)$, where ρ and φ are the normalized radial and azimuthal coordinates, then let the measured wavefront fitted to the first J Zernike functions, excluding piston, be

$$W^*(\rho, \varphi) = \sum_{j=2}^J c_j \cdot Z_j(\rho, \varphi). \quad (1)$$

The AOS controller input is then the vector of Zernike coefficients, \mathbf{c} , and we desire an output vector, \mathbf{d} , containing coefficients for Zernike tilt, focus, and coma, and P bending modes, which will minimize the alignment and figure errors present in the system.

$$\mathbf{c} = \begin{bmatrix} c_2 \\ \vdots \\ c_J \end{bmatrix} \quad (2)$$

$$\mathbf{d} = \begin{bmatrix} c'_2 \\ c'_3 \\ c'_4 \\ c'_7 \\ c'_8 \\ b_0 \\ \vdots \\ b_{P-1} \end{bmatrix} \quad (3)$$

The Zernike focus and coma coefficients, $c'_{4,7,8}$, are generally multiplied by sensitivity factors, calculated for the particular optical system, to determine collimation adjustments. The bending mode coefficients, $b_{0,P-1}$, are conventionally used to generate a mirror support force suite, based on a linear combination of force distributions for each mode. Note, that while wavefront tilt is typically corrected by a separate guiding system, it is needed for the conversion process unless care is taken to define all other Zernikes and bending modes as tilt-free over the system aperture. E.g. Zernike coma has some correlation with tilt over the typical annular telescope aperture.

Given the system inputs and outputs, we accordingly seek to define the conversion matrix, M , such that

$$M\mathbf{c} = \mathbf{d}. \quad (4)$$

3.2 Conversion Matrix

We begin the procedure of determining the elements of the conversion matrix by examining the components of the delivered wavefront. The wavefront is composed of contributions from controllable alignment and figure errors, and uncontrollable errors, such as atmospheric seeing, high-order figure errors and optical aberrations. The alignment contributions are represented by Zernike functions, while the controllable figure errors are represented by the first P bending mode functions, $B_p(\rho, \varphi)$, in order of increasing modal stiffness. The uncontrollable terms are lumped together and represented as $W_{junk}(\rho, \varphi)$, and the combined wavefront is then

$$W(\rho, \varphi) = \sum_{j=2,3,4,7,8} c'_j \cdot Z_j(\rho, \varphi) + \sum_{p=0}^{P-1} b_p \cdot B_p(\rho, \varphi) + W_{junk}(\rho, \varphi). \quad (5)$$

The measured and reported wavefront reduces each component to a best fit representation by Zernikes, indicated by an asterisk, and introduces an additional measurement error term, $W_\varepsilon^*(\rho, \varphi)$, so

$$W^*(\rho, \varphi) = \sum_{j=2,3,4,7,8} c'_j \cdot Z_j(\rho, \varphi) + \sum_{p=0}^{P-1} b_p \cdot B_p^*(\rho, \varphi) + W_{junk}^*(\rho, \varphi) + W_\varepsilon^*(\rho, \varphi). \quad (6)$$

The reduced bending mode representation, B^* , is defined to minimize the squared slope error integrated over the telescope aperture, S , such that

$$B_p^*(\rho, \varphi) = \sum_{j=2}^J a_{j,p} \cdot Z_j(\rho, \varphi), \text{ where} \quad (7)$$

$$\frac{\partial}{\partial a_{j,p}} \iint_S \left\| \nabla B_p(\rho, \varphi) - \sum_{i=2}^J a_{i,p} \cdot \nabla Z_i(\rho, \varphi) \right\|^2 \cdot d\rho \cdot d\varphi = 0, \quad \begin{matrix} j = 2, \dots, J \\ p = 0, \dots, P-1 \end{matrix}. \quad (8)$$

Although shown as a continuous integral, mirror bending modes are usually determined by finite element method at discrete locations on a surface node mesh, so the coefficients for minimum squared error may be determined by singular value decomposition.

Combining equations (1), (6) and (7), and omitting the uncontrollable terms, which will be addressed later as noise, we then have

$$\sum_{j=2}^J c_j \cdot Z_j(\rho, \varphi) = \sum_{j=2,3,4,7,8} c'_j \cdot Z_j(\rho, \varphi) + \sum_{p=0}^{P-1} b_p \cdot \sum_{j=2}^J a_{j,p} \cdot Z_j(\rho, \varphi). \quad (9)$$

This relation must be satisfied independently for each Zernike, producing the following set of equations:

$$c_j = \begin{cases} c'_j + \sum_{p=0}^{P-1} b_p \cdot a_{j,p}, & j = 2, 3, 4, 7, 8 \\ \sum_{p=0}^{P-1} b_p \cdot a_{j,p}, & j = 5, 6, 9, \dots, J \end{cases}. \quad (10)$$

These equations may be expressed in matrix form as

$$\mathbf{c} = N\mathbf{d}, \text{ where} \quad (11)$$

$$N = \begin{bmatrix} 1 & 0 & 0 & 0 & 0 & a_{2,0} & \cdots & a_{2,P-1} \\ 0 & 1 & 0 & 0 & 0 & 0 & \cdots & 0 \\ 0 & 0 & 1 & 0 & 0 & 0 & \cdots & 0 \\ 0 & 0 & 0 & 0 & 0 & 0 & \cdots & 0 \\ 0 & 0 & 0 & 0 & 0 & 0 & \ddots & \vdots \\ 0 & 0 & 0 & 0 & 0 & 0 & \ddots & \vdots \\ 0 & 0 & 0 & 1 & 0 & 0 & \cdots & 0 \\ 0 & 0 & 0 & 0 & 1 & 0 & \cdots & 0 \\ 0 & \cdots & 0 & 0 & 0 & 0 & \cdots & 0 \\ \vdots & \ddots & \vdots & 0 & 0 & 0 & \cdots & 0 \\ 0 & \cdots & 0 & a_{J,0} & 0 & 0 & \cdots & a_{J,P-1} \end{bmatrix}. \quad (12)$$

The matrix N is generally rectangular, and hence non-invertable, but the Moore-Penrose pseudo-inverse provides a conversion matrix which best-fits the output to the input in a least-squares sense, thus

$$M = N^+. \quad (13)$$

3.3 Matrix Size Considerations

The conversion matrix dimensions are, of course, equal to the input and output vector lengths, which are important parameters in the AOS system design. We provide here some constraints and recommendations on those dimensions.

The most obvious constraint is that input vector must have at least as many terms as the output vector, such that

$$J \geq P + 5. \quad (14)$$

Additionally, the set of input Zernike polynomials used must include the same range of azimuthal orders as the output bending modes. Both Zernike polynomials and bending modes have separable forms composed of a radial function and a harmonic azimuthal function, so terms with differing azimuthal orders are orthogonal. In practice, to avoid high noise sensitivity, the Zernike set should include at least one additional term for each azimuthal order, and two additional terms for orders 0 and 1 due to the presence of coma and focus in the output vector. By inspection of the azimuthal and radial

orders of the bending modes used for figure control, shown in Figure 2, one can determine sensible Zernike ranges to fit these shapes. E.g. the 26 DCT bending mode shapes include azimuthal orders up to $m=8$, requiring the inclusion of Zernikes 44 & 45 (the lowest terms with order $m=8$). Inclusion of ever-higher radial orders may continue to improve performance, so the information shouldn't be arbitrarily discarded, but offered very diminishing returns in the case of the DCT system.

Arranged in order of increasing modal stiffness, the bending mode shapes possess a corresponding increase in their characteristic spatial frequency. Thus, a finite set of modes serves as a low-pass spatial filter, with the cut-off frequency increasing with additional terms. This filtering limits the information, both signal and noise, passed from the wavefront sensor to the figure control system. The inherent mechanical stiffness of the mirror attenuates high-frequency errors due to external disturbance forces (although not errors due to figuring, CTE inhomogeneity, etc..), so above some frequency the measured noise will exceed the actual errors present in the system to the detriment of performance. This suggests there is an optimal number of bending modes to control depending on the relative mechanical errors vs. measured wavefront noise. The spatial and temporal characteristics of both the errors and noise are complex, and optimality doubly so, but given the potential to determine static errors very accurately (by shop testing or averaging down operational measurement noise) it may be worth addressing static and temporal errors separately.

A special consideration is confusion between the low-order Zernikes (focus & coma) used for collimation control and the analogous bending modes of the same radial and azimuthal orders. These modes are highly correlated (e.g. slope correlations for the DCT mirror are 0.96 and 0.93 for focus and coma, respectively, and their analogous modes), so care must be taken to avoid an ill-conditioned matrix; by increasing input Zernike terms or eliminating output bending modes, if necessary.

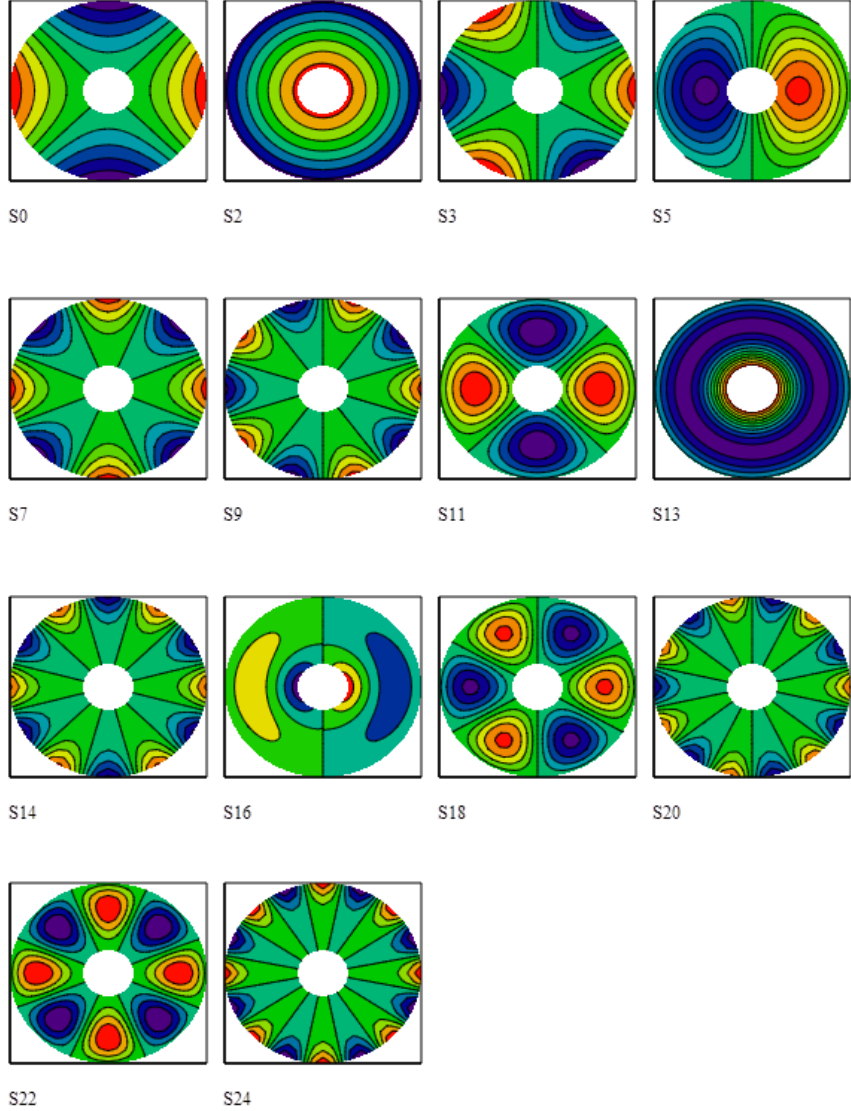


Figure 2. Approximate bending modes for the DCT primary mirror, only even modes shown.

3.4 Noise Sensitivity

To determine the number of bending modes to be controlled, it is useful to examine the expected noise in the system. If the noise, $W_{junk}^*(\rho, \varphi) + W_\epsilon^*(\rho, \varphi)$, can be characterized in terms of Zernike coefficients, \mathbf{c}_ϵ , then it is straightforward to determine the resulting force noise that the system will impose on the mirror. If $F_{p,n}$ is the force applied to an actuator, n of N , to induce a micron RMS wavefront displacement of mode shape p , then we can define a modal stiffness vector as

$$\mathbf{k} = \begin{bmatrix} k_0 \\ \vdots \\ k_{p-1} \end{bmatrix}, \text{ where} \quad (15)$$

$$k_p = \sqrt{\frac{1}{N} \sum_{n=1}^N (F_{p,n})^2}. \quad (16)$$

For a given input noise, the resulting vector of RMS force per bending mode is then

$$\mathbf{f}_\varepsilon = (M \mathbf{c}_\varepsilon) \mathbf{k}^T. \quad (17)$$

The examples below show the noise resulting from measurement error only, $W_\varepsilon^*(\rho, \varphi)$, for the DCT active optics system. The wavefront sensor is tasked with delivering Zernikes 2-47, with a combined slope accuracy of 0.012 arcseconds RMS. We assume the slope error is distributed even among the 46 Zernike terms, and convert from slope to displacement, so the error coefficients are then

$$c_{\varepsilon_j} = \frac{0.012'' \text{ RMS}}{\sqrt{46}} \cdot \frac{\iint_S Z_j(\rho, \varphi)^2 \cdot d\rho \cdot d\varphi}{\iint_S \|\nabla Z_j(\rho, \varphi)\|^2 \cdot d\rho \cdot d\varphi}. \quad (17)$$

Controlling the first 26 bending modes (0..25), this results in a total of 1.1N RMS force error, distributed as shown in Figure 3a. It is apparent that confusion with focus and coma causes high error forces for modes of azimuthal order 0 and 1 (i.e. modes 2, 5, 6, 13, 16 & 17). By dropping modes 13, 16 & 17 from the solution, the total force noise is reduced significantly to 0.6N RMS, distributed as shown in Figure 3b. Limiting the solution to only modes 0..12 reduces the total force noise to 0.17N, which compares favorably with the mechanical force error per actuator of ~0.25N RMS.

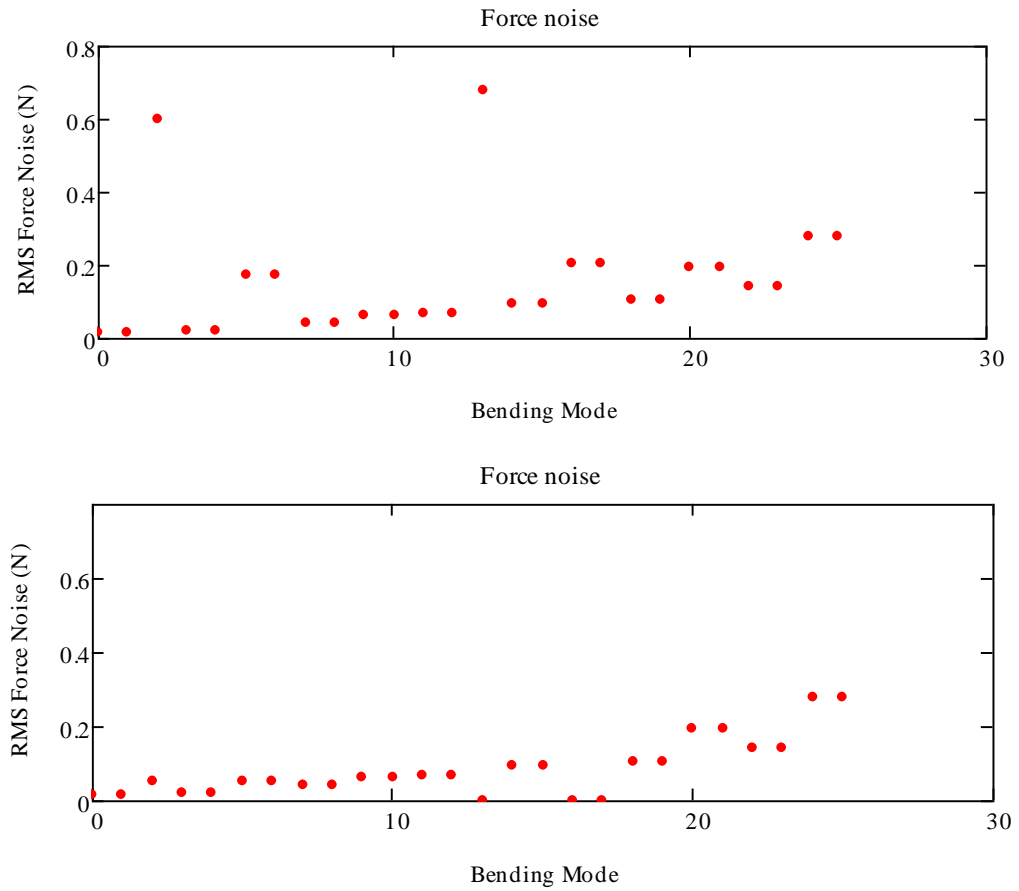


Figure 3. Measurement force noise for the DCT active optics system. Top includes all modes 0..25, bottom excludes modes 13, 16 & 17 from the fit solution.

4. CONCLUSIONS

The initial question we set out to address was: does the performance improvement of using bending modes, rather than Zernikes, for the basis of mirror figure control warrant the additional complexity associated with their use. Based on the performance analysis we can conclude that bending modes do perform significantly better than Zernikes as basis functions for control of thin meniscus mirrors. Given the demanding performance requirements of modern telescopes, the magnitude of the improvement is compelling. The surface slope difference shown in Table 1 corresponds to an image degradation contribution of 0.1 arc-sec FWHM, compared to a total system budget for the DCT of 0.25 arc-sec FWHM. Further, any additional complexity of using bending modes can be encapsulated in a simple transformation matrix developed in the design phase, and need not complicate system interfaces.

Thus, it is possible to achieve improved performance with bending modes at a very modest cost in complexity.

ACKNOWLEDGEMENTS

The author thanks Chen Liang, of the National Solar Observatory, and Alex Venetiou, of Lowell Observatory, for insightful conversation leading to the development of this paper.

REFERENCES

- [1] Noll, R.J., "Zernike polynomials and atmospheric turbulence," *J. Opt. Soc. Am.*, Vol. 66, No.3, (1976).
- [2] Noethe, L., "Active optics in Modern, Large Optical Telescopes," *Progress in Optics*, Vol. 43, (2002).
- [3] Smith, B.W., Chylek, T., Cuerden, B., DeGroff, B., Lotz, P.J. and Venetiou, A. "The active optics system for the Discovery Channel Telescope," *Proc. SPIE* 7739-63 (2010).
- [4] Schechter, P.L., Burley, G.S., Hull, C.L., Johns, M., Martin, H.M., Schaller, S., Shectman, S.A. and West S.C., "Active Optics on the Baade 6.5-m (Magellan I) Telescope," *Proc. SPIE* 4837 (2003).